Anal. Bioanal. Electrochem., Vol. 17, No. 5, 2025, 390-413
https://www.doi.org/10.22034/abec.2025.724934

Analytical & Bioanalytical Electrochemistry

Full Paper

Synthesis and Evaluation of Hollow Structured Gd-Co-N-PC Electrocatalysts Originating from MOFs for Effective Oxygen Reduction Reaction

Zeinab Kebriaei,[1] Mehdi Mehrpooya,[1,2,*] Javad Kouhsorkhi,[3] Seyed Ali Mousavi,[4] and Farshad Torabi[5]

[1]*School of Energy Engineering and Sustainable Resources, College of Interdisciplinary Science and Technology, University of Tehran, Tehran, Iran*
[2]*Hydrogen and fuel cell laboratory, University of Tehran, Tehran, Iran*
[3]*Advanced Micro and Nano Fabrication Devices Lab, Department of MEMS and NEMS, School of Intelligent, University of Tehran, Tehran, Iran*
[4]*School of Mechanical Engineering, Shiraz University, Shiraz, Iran*
[5]*Battery and Energy Generator Research Lab, K.N. Toosi University of Technology, Iran*

*Corresponding Author, Tel.: +98(21)88497167
E-Mail: mehrpoya@ut.ac.ir

Received: 21 March 2025 / Received in revised form: 23 May 2025 / Accepted: 25 May 2025 / Published online: 31 May 2025

Abstract- Platinum remains the predominant catalyst for the oxygen reduction reaction (ORR) occurring at both the cathode and anode in fuel cells and metal–air batteries; however, its elevated expense, shortage, and restricted consistency in alkaline environments hinder widespread commercialization. To overcome these constraints, this research emphasizes the creation and assessment of a novel multimetallic electrocatalyst obtained from metal–organic frameworks (MOFs) and stabilized with a silicate coating. A hollow-structured catalyst was prepared by carbonizing ZIF-8@Gd-ZIF-67@SiO_2, with mesoporous silica ($mSiO_2$) applied to prevent particle aggregation during high-temperature pyrolysis. The integration of carbon frameworks, metal doping, and silica protection effectively enhanced the structural integrity and catalytic performance. Detailed physical and electrochemical studies showed that the newly developed electrocatalysts had a consistent shape, nanoscale particle sizes, and high surface areas. Compared to commercial Pt/C (20%), the Gd-Co-N-PC electrocatalyst achieved an onset potential of –0.12 V and an electron transfer count of 3.69, suggesting a near-four-electron ORR pathway and superior catalytic activity. Stability tests further confirmed its excellent durability under operational conditions. Overall, the developed electrocatalysts offer a promising, cost-effective alternative to platinum-based materials for fuel cell applications, combining high ORR efficiency with robust structural stability for future energy conversion technologies.

Keywords- Oxygen Reduction Reaction; Metal–Organic Frameworks; Multimetallic Electrocatalysts; Silica Coating; Fuel Cells

1. INTRODUCTION

With the world's population expanding swiftly, the need for energy also rises that's both clean and sustainable putting increased pressure on global energy resources. Simultaneously, the environmental toll of conventional energy use, especially the steady rise in greenhouse gases like CO_2, has brought climate change and ecological degradation into sharp focus. These challenges have made it clear that new approaches to producing and storing energy are urgently needed. In response, researchers across the globe are working intensively to develop innovative technologies that are not only environmentally responsible but also efficient and economically feasible. Technologies that convert and store energy through electrochemical methods—like fuel cells, metal–air batteries [1], and supercapacitors have gained significant attention as promising alternatives. Their main advantage lies in the direct conversion of chemical energy into electricity, all while keeping environmental harm to a minimum [2,3]. Among these, fuel cells are especially appealing due to their elevated energy conversion efficiency, minimal pollutant emissions, and diverse applications spanning transportation, stationary power generation, and portable electronic devices.

Fuel cells operate through electrochemical reactions at the electrodes, converting the chemical energy of fuels into electricity. Polymer electrolyte membrane fuel cells (PEMFCs) have attracted considerable scholarly interest owing to their reduced operational temperatures. (approximately 60–80 °C) [4], high power densities, and rapid start-up times, making them promising candidates to replace internal combustion engines, especially in automotive applications. Despite these advantages, challenges such as the high cost and limited durability of catalyst materials continue to restrict their large-scale commercialization. The membrane electrode assembly (MEA) consists of the membrane that conducts protons [5], gas diffusion layers [6], catalyst layers, and backing layers are the core component of PEMFCs [7]. Catalyst layer optimization is critical for improving overall fuel cell performance, durability, and cost-effectiveness. Currently, platinum (Pt) and its alloys are the benchmark catalysts for reactions at both the anode and cathode in fuel cells, due to their exceptional catalytic effectiveness for the hydrogen oxidation reaction (HOR) and oxygen reduction reaction (ORR) [8]. PtRu/C catalysts are used at the anode to mitigate carbon monoxide poisoning, while Pt/C catalysts are preferred at the cathode for their excellent ORR activity. However, the high cost, limited abundance, and susceptibility of platinum catalysts to degradation, especially in alkaline environments, severely constrain the economic viability of fuel cell technologies. Thus, reducing platinum loading while maintaining high catalytic efficiency remains a major research objective in fuel cell development.

To address this, extensive research has focused on developing noble-metal-free and multimetallic catalysts based on earth-abundant elements. Transition metals like cobalt (Co), iron (Fe), and manganese (Mn) are known to have been widely studied for enhancing ORR activity when incorporated into carbon-based matrices. However, achieving performance comparable to platinum-based catalysts regarding both performance and durability remains challenging. Metal-organic frameworks (MOFs) have recently emerged as promising candidates for the creation of sophisticated electrocatalysts. These structures, made up of metal ions or clusters connected by organic linkers, are known for their exceptionally high surface areas, adjustable porosity, and flexible architecture. These features make MOFs excellent templates for producing nanostructured catalysts that offer a rich supply of active sites, better mass transport, and greater structural stability, key qualities for high-performance electrochemical applications [9].

Among MOFs, zeolitic imidazolate frameworks (ZIFs), including ZIF-8 (comprised of Zn^{2+} and 2-methylimidazole) [10] and ZIF-67 (comprised of Co^{2+} and 2-methylimidazole) [11], have demonstrated particular promise in electrocatalysis [12,13]. Their exceptional chemical stability, tunable morphology, and facile synthesis render them highly promising candidates for catalyst development [14,15].The catalytic efficacy of MOF-derived structures can be further enhanced through heteroatom doping (e.g., nitrogen, sulfur, phosphorus) and the incorporation of additional metallic elements, resulting in the formation of multimetallic active centers. Moreover, core–shell architectures, where one MOF encapsulates another, significantly improve conductivity, surface area, and catalytic enhancement due to synergistic interactions. Accordingly, extensive research into ZIF- and MOF-based electrocatalysts for the oxygen reduction reaction (ORR) has been carried out, drawing substantial global interest. Zirui Jia et al. [16]demonstrated that porous carbon structures could be synthesized from ZIF precursors using a calcination approach under controlled decoration conditions. A. Mousavi et al. [17] developed nitrogen- and sulfur-doped reduced graphene oxide (NS-RGO) incorporated into Cu-MOF structures. Among the studied samples, the 8% NS-RGO-Cu-MOF exhibited superior ORR performance, with an onset potential of -0.06 V versus Ag/AgCl. Binling Chen and colleagues [18] identified ZIF-67 and ZIF-8 as common precursors for ORR catalysts, which, upon pyrolysis under inert atmospheres (Ar or N_2), can be converted into carbon/metal oxide composites with organic ligands. Esmaili et al. [19] proposed a bifunctional electrocatalyst platform for both supercapacitor and reduction applications. The innovation of their study lies in the synthesis route and the electrochemical behavior of the resultant materials. This approach utilizes ZIF-8, ZIF-67, and MIL-101 as precursors to fabricate three classes of electrocatalysts, followed by the incorporation of Cu, Ce, and La dopants to enhance conductivity and structural stability. Linear sweep voltammetry (LSV) results revealed an onset potential of 0.064 V (*vs.* Ag/AgCl) for CoZn@NC, with an electron transfer number of 3.64. Bakhtavar et al. [20] introduced a novel

composite, Co@NC/GCN50-CNT20, consisting of GCN, CNT, and Co derived from ZIF-8@ZIF-67. The synergistic interaction among these constituents significantly augmented catalytic activity, leveraging their distinct morphologies, heterogeneous interfaces, and mechanical robustness. The composite displayed excellent ORR activity with an onset potential of -0.07 V. Zhimin Zhou [21] synthesized a rare-earth metal–organic framework (Gd-MOF) from $GdCl_3$ and pyromellitic dianhydride in N,N-dimethylformamide. This material functioned as a heterogeneous catalyst for de-alcoholization reactions to generate β-alkoxy alcohols. Similarly, Sachin Kumar and associates [22] developed lanthanide-based double oxide perovskites via a citrate–nitrate sol–gel technique. These materials exhibited dual catalytic behavior for both the oxygen evolution reaction (OER) and ORR, with Gd-containing compositions demonstrating optimal activity. Mousavi et al. [23] proposed a methodology leveraging rare-earth cation doping (Gd, Eu, Sm) to enhance the electrocatalytic activity of ZIF-8 for ORR. The observed performance enhancement is attributed to the distinct redox characteristics, improved conductivity, and specific electronic configurations of the lanthanide elements. The individual effects of Gd, Eu, and Sm on ORR vary due to differences in their electronic structures and roles within the ZIF-8 framework. Nevertheless, challenges such as structural degradation and nanoparticle agglomeration during pyrolysis remain prevalent. To address these issues, numerous studies have incorporated protective layers, particularly mesoporous silica (SiO_2). In this context, an $mSiO_2$ shell envelops the precursor material prior to pyrolysis, thereby maintaining structural integrity, preventing nanoparticle sintering, and facilitating the formation of hollow carbon architectures to improve catalytic performance. Shang et al. [24] demonstrated that $mSiO_2$ coatings are instrumental in mitigating nanoparticle agglomeration during thermal treatment. They fabricated porous carbon materials from ZIFs using this protective strategy, particularly in Zn-Co-ZIF composites. In another study, Hamed Kamali et al. [25] investigated the electrochemical benefits of applying $mSiO_2$ encapsulation on CuFe-ZIF-based materials for both ORR and supercapacitor applications. Their findings showed an improved onset potential of -0.04 V vs. Ag/AgCl and an average electron transfer number of 3.55, indicating a favorable 4-electron pathway. Mousavi et al. [26] introduced a multifunctional catalyst, Cu@Fe–N–C@MXene, for ORR, water splitting, and energy storage applications. The pivotal innovation in their work was the application of an $mSiO_2$ protective shield, which effectively suppressed sintering and maintained the structural and catalytic integrity of the Cu@Fe–N–C architecture during high-temperature pyrolysis (920 °C).

In this work, a new strategy was developed to create multimetallic electrocatalysts by integrating metal–organic frameworks (MOFs) with a protective layer of mesoporous silica. The process began with the hydrothermal synthesis of ZIF-8, which was then modified by introducing ZIF-67 and gadolinium (Gd^{3+}) ions to form a core–shell structure known as ZIF-8@Gd-ZIF-67. To preserve its structure during heat treatment, the composite was coated with a thin layer of silica before undergoing controlled pyrolysis. This resulted in the formation of

hollow Gd-Co-N-doped carbon (Gd-Co-N-PC) electrocatalysts featuring an extensive surface area, abundant active sites, and enhanced electrical conductivity [27].

The primary objective of this research is to develop efficient, long-lasting, and affordable multimetallic electrocatalysts that can serve as viable alternatives to platinum-containing substances for the oxygen reduction reaction (ORR) in fuel cells. By combining the structural advantages of MOF-derived frameworks, the enhanced reactivity from multimetallic doping, and the stability provided by a silica coating, this work seeks to address key issues such as catalyst degradation, particle aggregation, and performance decline ultimately supporting the development of more sustainable energy conversion technologies.

2. EXPERIMENTAL SECTION

This study presents the development of a nanocomposite electrocatalyst designed to tackle the ongoing challenges posed by the high cost and limited availability of platinum-based catalysts in fuel cell technology. The material features a polyhedral carbon structure infused with multiple metals, derived from a zeolitic imidazolate framework (ZIF). The overarching aim was to create a catalyst that is not only efficient and long-lasting but also more economical to produce.

ZIF-8 was initially synthesized using a hydrothermal method and subsequently functionalized through the growth of a core–shell structure with ZIF-67 and gadolinium (Gd^{3+}) to enhance electron transfer and increase surface area. The resulting ZIF-8@Gd-ZIF-67 composite was then subjected to pyrolysis, yielding a Gd-Co/NCNHP material with a nitrogen-doped carbon framework. Although the resulting three-dimensional tunable carbon structure exhibited a large surface area and abundant nitrogen sources both critical for the formation of active catalytic sites issues such as particle aggregation during pyrolysis and the dominance of microporous structures limited the exposure of active sites and hindered electrolyte diffusion. Consequently, developing improved strategies to mitigate aggregation and optimize mass transport within MOF-derived carbon materials remains essential. To address these issues, the ZIF-8@ZIF-67 composite was further enhanced by incorporating gadolinium and applying a mesoporous silica ($mSiO_2$) coating. This silica layer acted as a protective barrier during the pyrolysis process, helping to preserve the structure and support the formation of a hollow, polyhedral nitrogen-doped carbon framework embedded with cobalt and gadolinium species.To assess the structure and performance of the resulting electrocatalysts, a range of physical and electrochemical characterization techniques was employed. These results were then in comparison to the commercial 20% Pt/C catalyst to assess advancements in catalytic activity and the potential for practical fuel cell applications.

2.1. Materials

All chemicals employed in this study were of analytical grade and were used as received, without any additional purification. The materials included zinc nitrate hexahydrate ($Zn(NO_3)_2 \cdot 6H_2O$), cobalt nitrate hexahydrate ($Co(NO_3)_2 \cdot 6H_2O$), gadolinium nitrate hexahydrate ($Gd(NO_3)_3 \cdot 6H_2O$), tetraethyl orthosilicate (TEOS), 2-methylimidazole, ethanol, ammonium hydroxide solution (25–28%), and hydrofluoric acid (3 wt%). All reagents were commercially sourced. Deionized (DI) water was used in all experimental steps (see Table 1 for details).

Table 1. Raw materials used in the fabrication of electrocatalysts for the oxygen reduction reaction

No.	Material	Manufacturer	Purpose of Use
1	5% Nafion Solution	Dupont	Polymer used in catalyst fabrication
2	2-Methylimidazole ($C_4H_6N_2$)	Merck	Ligand in the synthesis of the zeolitic imidazolate framework
3	Cobalt Nitrate Hexahydrate ($Co(NO_3)_2 \cdot 6H_2O$)	Merck	Synthesis of zeolitic imidazolate framework
4	Zinc Nitrate Hexahydrate ($Zn(NO_3)_2 \cdot 6H_2O$)	Merck	Synthesis of zeolitic imidazolate framework
5	Gadolinium Nitrate	Merck	Synthesis and fabrication of the composite
6	Ammonia Solution (NH_4OH)	Merck	Synthesis of silica nanospheres
7	Tetraethyl Orthosilicate ($Si(OC_2H_5)_4$)	Merck	Synthesis of silica nanospheres
8	Polyvinylidene Fluoride (PVDF)	-	Fabrication of working electrode for CV and GCD tests
9	Carbon Black	-	Fabrication of working electrode for CV and GCD tests
10	N-Methylpyrrolidone (NMP)	-	Fabrication of working electrode for CV and GCD tests
11	Potassium Hydroxide (KOH) Solution (1 M)	-	Fabrication of working electrode for CV and electrochemical tests
12	Nickel Foam	-	Fabrication of working electrode for CV and GCD tests
13	Deionized Water (H_2O)	-	Washing steps
14	Ethanol (C_2H_5OH)	-	Washing steps
15	Methanol (CH_3OH)	Merck	Washing steps
16	Hydrofluoric Acid (HF)	Merck	Washing steps
17	Paraffin Oil	-	Oil bath for thermal treatment
18	Silicone Oil	-	Oil bath for thermal treatment

2.2. Synthesis Procedures

In this study, silica nanospheres were synthesized using a modified version of the Stöber method. Initially, a mixture of 325 mL of ethanol and 125 mL of deionized water was stirred for 15 minutes. Subsequently, 22.5 mL of tetraethyl orthosilicate (TEOS) was added under vigorous stirring, which continued for another 15 minutes. Then, 45 mL of ammonium

hydroxide solution was introduced, and the reaction was maintained at room temperature (approximately 25 °C) for 12 hours. The resulting colloidal silica was isolated through centrifugation at 5000 rpm for 10 minutes, rinsed three times with ethanol and deionized water, and dried in a vacuum oven at 70 °C (Figure 1-A). To synthesize ZIF-8, 5.95 g of zinc nitrate hexahydrate and 16.6 g of 2-methylimidazole were separately dissolved in 150 mL of methanol and subjected to ultrasonication for 30 minutes to ensure complete dissolution [28]. The 2-methylimidazole solution was then slowly added to the zinc nitrate solution under continuous stirring, and the resulting mixture was stirred at room temperature for 24 hours. The resulting precipitate was collected by centrifugation, washed thoroughly with methanol, and dried under vacuum at 60 °C [23,24] (Figure 1-A). For the fabrication of the core–shell structure ZIF-8@Gd-ZIF-67, 0.5 g of ZIF-8 was dispersed in 100 mL of methanol (solution 1). Separately, 4.08 g of cobalt nitrate hexahydrate and 1.74 g of gadolinium nitrate hexahydrate were dissolved in another 100 mL of methanol (solution 2), and 16.6 g of 2-methylimidazole was dissolved in a third 100 mL of methanol (solution 3) (Figure 1-B). Solution 2 was added to solution 1 under stirring to form a homogeneous mixture (solution 4), followed by the addition of solution 3. This final mixture was stirred at 25 °C for 24 hours. The resulting solid was separated by centrifugation at 5000 rpm for 10 minutes, rinsed with methanol, and dried under vacuum at 60 °C overnight (Figure 1-C). For the silica coating process, 2.0 g of ZIF-8@Gd-ZIF-67 was dispersed in 20 mL of methanol and stirred for 15 minutes. Then, 1.0 g of the previously synthesized silica nanospheres was added, and the mixture was subjected to ultrasonication for 30 minutes. The dispersion was then stirred at 70 °C for 1 hour and dried under vacuum at 60 °C overnight. The dried ZIF-8@Gd-ZIF-67@SiO_2 composite was pyrolyzed in a tubular furnace under a nitrogen atmosphere. The temperature was increased gradually at a rate of 5 °C per minute until reaching 900 °C and maintained at that temperature for 2 hours [31].

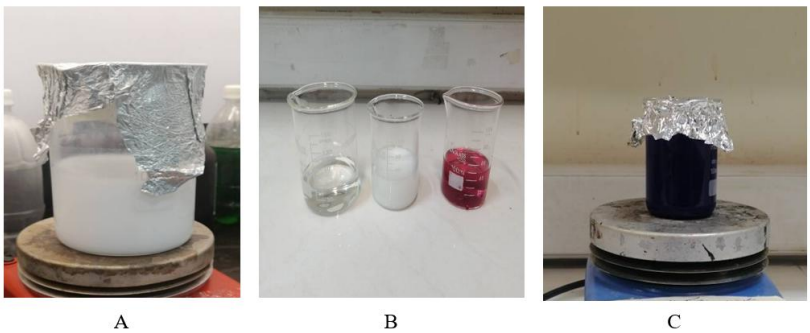

Figure 1. The procedure for producing the ZIF-8@Gd-ZIF-67

During pyrolysis, zinc was evaporated due to its low boiling point, a highly porous black carbonaceous structure was formed, and the density and uniformity of active sites were significantly enhanced. After cooling to room temperature, the resulting black powder was

treated with 3 wt% hydrofluoric acid (HF) at 60 °C for 2 hours to remove the silica template. The final product was extensively rinsed with deionized water and ethanol to eliminate any remaining HF and then dried under vacuum at 60 °C overnight, yielding the Gd-Co/NCNHP electrocatalyst.

2.3. Physical Characterization

To investigate the physical properties, structure, and morphology of the synthesized electrocatalysts, a series of characterization techniques was employed. emission scanning electron microscopy (SEM) and Field-emission scanning electron microscopy (FESEM) was employed to examine the morphology and surface characteristics of the samples under high vacuum conditions, with the column pressure maintained at 0.1 mbar and an acceleration voltage adjustable between 5–30 kV. Powder Specimens were covered with a thin layer of gold to enhance electrical conductivity and improve imaging resolution. Transmission electron microscopy (TEM) was employed to analyze the morphology, particle size, and internal structure of the materials, operating under high vacuum conditions with an accelerating voltage range of 80–300 kV. For TEM analysis, powder samples were dispersed in ethanol using ultrasonication and then drop-cast onto carbon-coated copper grids. X-ray diffraction (XRD) analysis was conducted to identify the compositions, crystalline phases, and crystal structures of the materials using a Cu Kα radiation source (λ = 1.5406 Å) over a scanning range of 2θ = 5°–100°, with powder samples uniformly pressed into flat sample holders[32]. Fourier-transform infrared (FTIR) spectroscopy was employed to identify the functional groups and chemical bonds present in the materials across the spectral range of 4000–400 cm^{-1}, using samples that were prepared by combining powder with potassium bromide (KBr)[33] and pressing them into transparent pellets. Raman spectroscopy was performed to evaluate chemical bonds and structural features using a Raman microscope equipped with a 514 nm laser source, operating within a spectral range of 100–4000 cm^{-1} and maintaining the laser power below 10 mW to prevent sample heating. For Raman analysis, powder samples were directly placed on clean glass slides [34].

2.4. Electrochemical Measurements

Electrochemical evaluations were performed to examine the electrochemical behavior, reaction kinetics, surface properties, and catalytic performance of the synthesized electrocatalysts, particularly in the oxygen reduction reaction (ORR). These measurements offer an understanding of the materials' catalytic efficiency and stability. All electrochemical studies were performed using an electrochemical workstation featuring a standard three-electrode arrangement, which includes a glassy carbon rotating disk electrode (RDE) measuring 5 mm in diameter, utilizing an Ag/AgCl (saturated KCl) reference electrode as the working electrode, along with a platinum wire counter

electrode. A 0.1 M aqueous solution of KOH, saturated with either oxygen (O_2) or argon (Ar) gas, was used as the electrolyte, and all measurements were conducted at ambient conditions (25 °C and 1 atm). The catalyst ink was prepared by dispersing 2 mg of catalyst powder in a 1:1 volumetric mixture of ethanol and deionized (DI) water, supplemented with 20 μL of 5 wt% Nafion® solution. This mixture was ultrasonicated for 1 hour to achieve a homogeneous dispersion, after which 10 μL of the ink was drop-cast onto the surface of the RDE and dried at room temperature. Several electrochemical techniques were employed: Cyclic voltammetry (CV) was conducted within a potential spans from –1.0 V to +0.2 V against Ag/AgCl at a scanning rate of 100 mV s^{-1} in O_2- or Ar-saturated 0.1 M KOH to evaluate the electrochemical behavior; linear sweep voltammetry (LSV) was conducted to assess ORR activity by recording the current response while linearly sweeping the range from 0.2 V to -1.0 V relative to Ag/AgCl at a scanning rate of 10 mV s^{-1}, with RDE rotation speeds varying between 400 and 2025 rpm to analyze mass transport effects, and the onset potential for ORR initiation was determined from the LSV curves, with more positive onset potentials indicating better ORR kinetics. Chronoamperometry tests were carried out to assess catalyst stability by using a constant voltage of –0.4 V for 1000 seconds in a 0.5 M KOH solution, continuously recording the current over time. Finally, Koutecky–Levich (K–L) analysis was employed to determine the electron transfer number (n), providing insight into whether the ORR followed a 2-electron or a more efficient 4-electron pathway. The K–L plots provide critical information regarding the reaction pathway and kinetic parameters of the catalysts. The responses of the aforementioned mechanisms can be articulated as follows [35]:

$$O_2 + 2\,H_2O + 4e^- \rightarrow 4\,OH^- \qquad E° = 0.401\ V \tag{1}$$

$$O_2 + H_2O + 2e^- \rightarrow HO_2^- + OH^- \qquad E° = 0.080\ V \tag{2}$$

$$HO_2^- + H_2O + 2e^- \rightarrow 3OH^- \qquad E° = 0.880\ V \tag{3}$$

By applying the Koutecky-Levich (K-L) equations, the electron transfer number (n) can be determined as[36,37]:

$$\frac{1}{J} = \frac{1}{J_K} + \frac{1}{B\omega^{0.5}} \tag{4}$$

$$\frac{1}{J} = \frac{1}{J_K} + \frac{1}{0 \cdot 62\ nFC_0(D_0)^{\frac{2}{3}}} v^{\frac{1}{6}} \omega^{0.5} \tag{5}$$

$$\omega = 2\pi N \tag{6}$$

$$B = 0 \cdot 62\ nFC_0(D_0)^{\frac{2}{3}} v^{\frac{-1}{6}} \tag{7}$$

As per the subsequent equations, J ($mA \cdot cm^{-2}$) indicates the recorded current density, whereas J_k ($mA \cdot cm^{-2}$) refers to the kinetic current density.

The symbol ω (rad·s^{-1}) represents the angular velocity of the working electrode. The variable n represents the quantity of electrons that are transferred per oxygen molecule during the reaction, and F (96.485 C·mol^{-1}) represents the Faraday constant. The parameter ν (0.01 cm^2·s^{-1}) denotes the kinematic viscosity of the electrolyte. Moreover, CO_2 (1.2×10^{-6} mol·cm^{-3}) denotes the overall concentration of dissolved oxygen in 0.1 M KOH, while D_O_2 (1.9×10^{-5} cm^2·s^{-1}) signifies the diffusion coefficient of oxygen in that same environment [38].

3. RESULTS AND DISCUSSION

The findings of this research highlight the encouraging potential of the synthesized Gd-Co-N-PC electrocatalyst as a budget-friendly and effective substitute for catalysts based on precious metals in the alkaline medium of the oxygen reduction reaction (ORR).

The hollow polyhedral morphology and interconnected three-dimensional carbon framework, as confirmed by SEM and FESEM, TEM, and Raman spectroscopy, provided an abundance of active sites and enhanced mass transport properties, both critical for improving ORR kinetics. The application of mesoporous silica as a protective shell during the pyrolysis process effectively prevented particle aggregation, preserving surface area and maximizing active site exposure. This strategy marks a significant advancement over conventional MOF-derived catalysts, which often suffer from structural collapse and performance degradation during high-temperature treatment. Electrochemical analyses revealed that the Gd-Co-N-PC catalyst exhibited an onset potential of –0.12 V and an electron transfer number of approximately 3.69, indicative of a near-complete four-electron pathway. These findings show catalytic performance similar to that of the commercial Pt/C 20% catalyst [39] but achieved using abundant and low-cost elements. The incorporation of gadolinium (Gd) not only enhanced electronic conductivity but also improved the thermal stability and oxidation resistance of the electrocatalyst, making it suitable for harsh operational conditions. The synergistic effect between cobalt and gadolinium further contributed to the enhanced durability and activity compared to single-metal systems. Chronoamperometry tests confirmed the excellent operational stability of the Gd-Co-N-PC catalyst, attributed to the robust carbon matrix and the effective dispersion of metal active sites throughout the framework. This superior stability is essential for practical fuel cell applications.

In summary, this research introduces a novel design approach that combines MOF-derived carbon structures with multimetallic doping and silica shielding, leading to an ORR catalyst that is exceptionally active, long-lasting, and cost-effective. These findings pave the way for further development of platinum-free catalysts for sustainable energy conversion and storage technologies. Future research directions include optimizing the metal ratios, exploring alternative dopants, and scaling up the synthesis process for practical deployment in fuel cells and metal–air batteries.

3.1. Physical Analysis of the Produced Catalysts

3.1.1. SEM and FESEM Analysis

The SEM analyses offered a detailed understanding of the morphological characteristics of the synthesized materials at various stages of the fabrication process. SEM images of SiO_2 nanospheres confirmed their successful synthesis via the modified Stöber method, demonstrating uniform spherical morphology, smooth surfaces, and excellent monodispersitycrucial features for ensuring homogeneous coatings in composite architectures. The micrographs of ZIF-8 revealed well-defined polyhedral crystals with nanometer-scale dimensions, indicative of the formation of a high-quality metal–organic framework (MOF) structure and favorable surface-to-volume ratio, beneficial for catalytic applications. Upon incorporation of cobalt and gadolinium into the structure, SEM images of the ZIF-8@Gd-ZIF-67 composite exhibited clearly defined dual-shelled nanocages, where an inner nitrogen-doped microporous carbon framework derived from ZIF-8 was surrounded by an outer mesoporous Co–NC shell originating from ZIF-67, together providing synergistic improvements in mass transport and electrical conductivity.

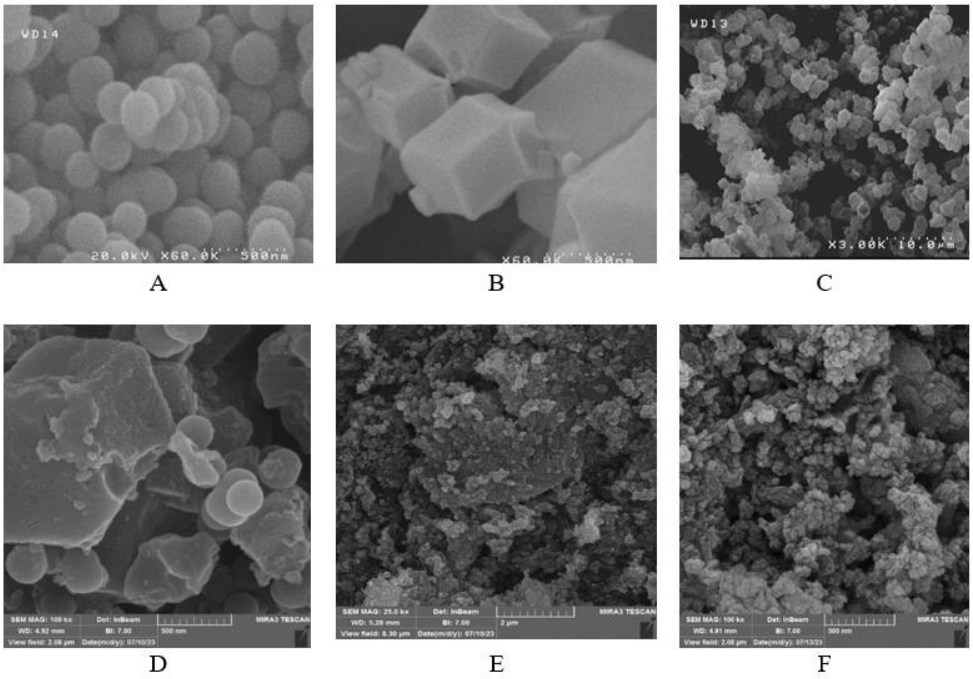

Figure 2. SEM and FESEM images for (A) SiO_2,(B) ZIF-8, (C) ZIF-8@Gd-ZIF-67, (D) ZIF-8@Gd-ZIF-67@SiO_2, (E) Gd-Co-N-PC after pyrolysis (before HF washing), and (F) Gd-Co-N-PC after HF washing

The application of a silica coating played a pivotal role in maintaining the structural integrity of the core–shell configuration during pyrolysis, ultimately yielding rhombic dodecahedral hollow nanocages with high porosity and reduced particle fusion. Post-pyrolysis

SEM characterization confirmed the evolution of hollow polyhedral morphologies, attributed to the evaporation of zinc and gas release during thermal treatment, which facilitated enhanced electron and mass transfer capabilities. Finally, after the removal of the silica template using HF, the resulting interconnected carbon network displayed hollow structures that generated abundant active three-phase interfaces, significantly contributing to improved oxygen reduction and evolution kinetics (Figure 2).

3.1.2. TEM and EDX Analysis

TEM images (Figure 3) revealed hollow polyhedral structures with dispersed Co and Gd nanoparticles embedded in the carbon matrix. EDX mapping (Figure 4,Figure **5**,6) confirmed the successful removal of silica and the even distribution of Co, Gd, C, and N elements, guaranteeing optimal exposure of active sites.

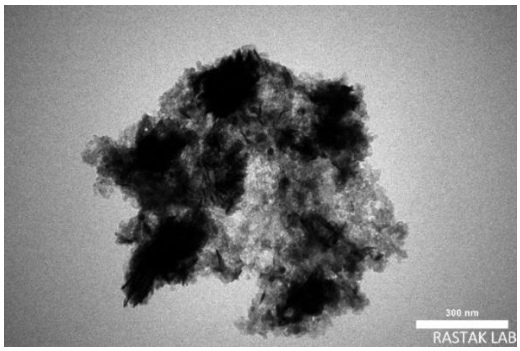

Figure 3. TEM images of the Gd-Co-N-PC electrocatalyst after HF washing, showing hollow polyhedral structures with embedded Co and Gd nanoparticles

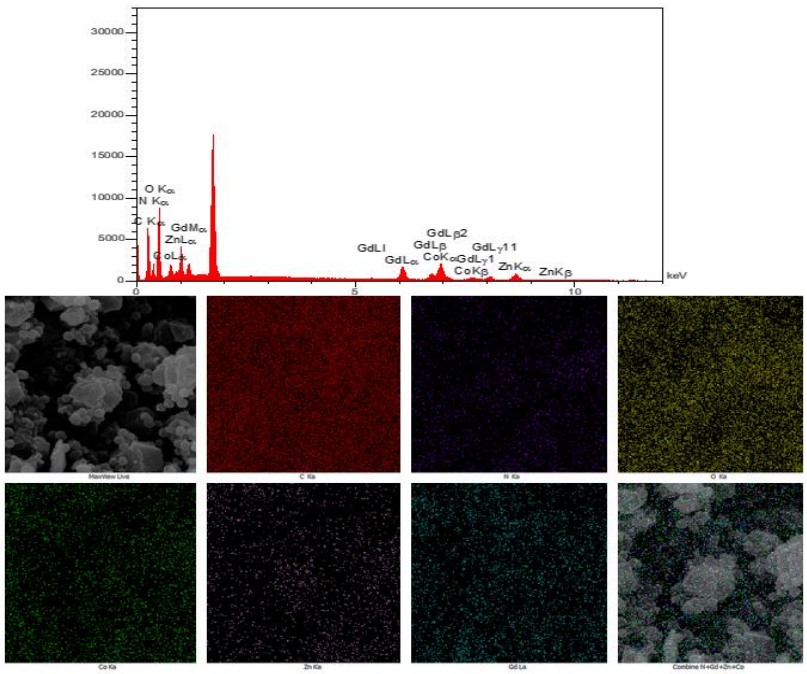

Figure 4. The EDS and elemental mapping analyses for the ZIF-8@Gd-ZIF-67@SiO_2

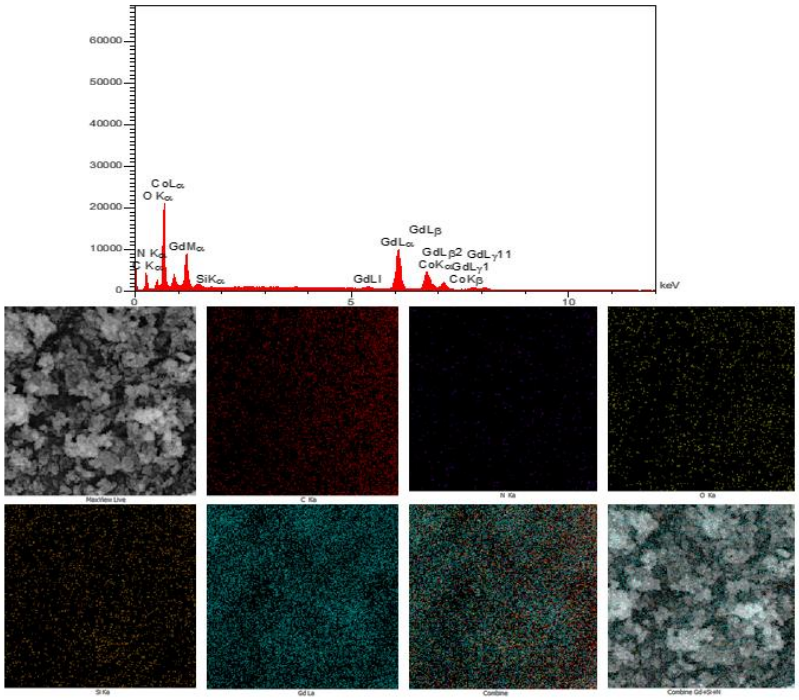

Figure 5. The EDS and elemental mapping analyses of the Gd-Co-N-PC following pyrolysis demonstrate the uniform distribution of carbon (C) and nitrogen (N) throughout the Gd-Co-N-PC structure post-silica removal

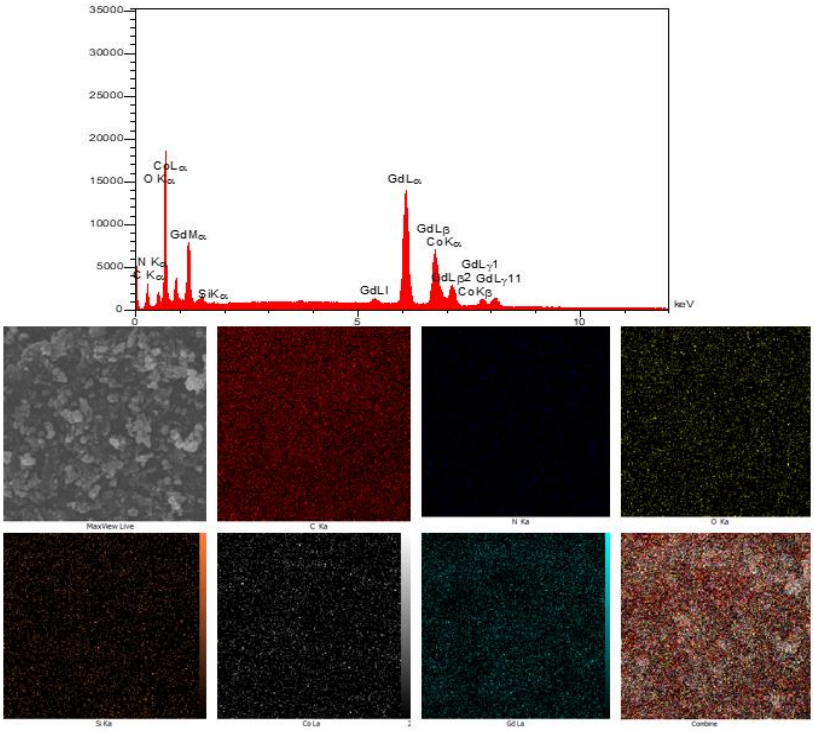

Figure 6. The EDS and elemental mapping analyses of the Gd-Co-N-PC after HF washing indicate the uniform distribution of Co, Gd, C, and N throughout the Gd-Co-N-PC structure following HF treatment

3.1.3. Structural Analysis via XRD

XRD patterns (Figure 7) demonstrated the successful synthesis of ZIF-8@Gd-ZIF-67 precursors, as evidenced by sharp diffraction peaks. After pyrolysis, peaks corresponding to graphitic carbon (002 plane) and metallic cobalt (FCC structure) appeared, confirming the transformation into a carbon-based metallic catalyst. The absence of Zn peaks indicated its complete removal during thermal treatment, enhancing the catalytic surface purity.

The presence of the (111) plane in cobalt nanoparticles is significant, as it correlates with excellent ORR catalytic activity.

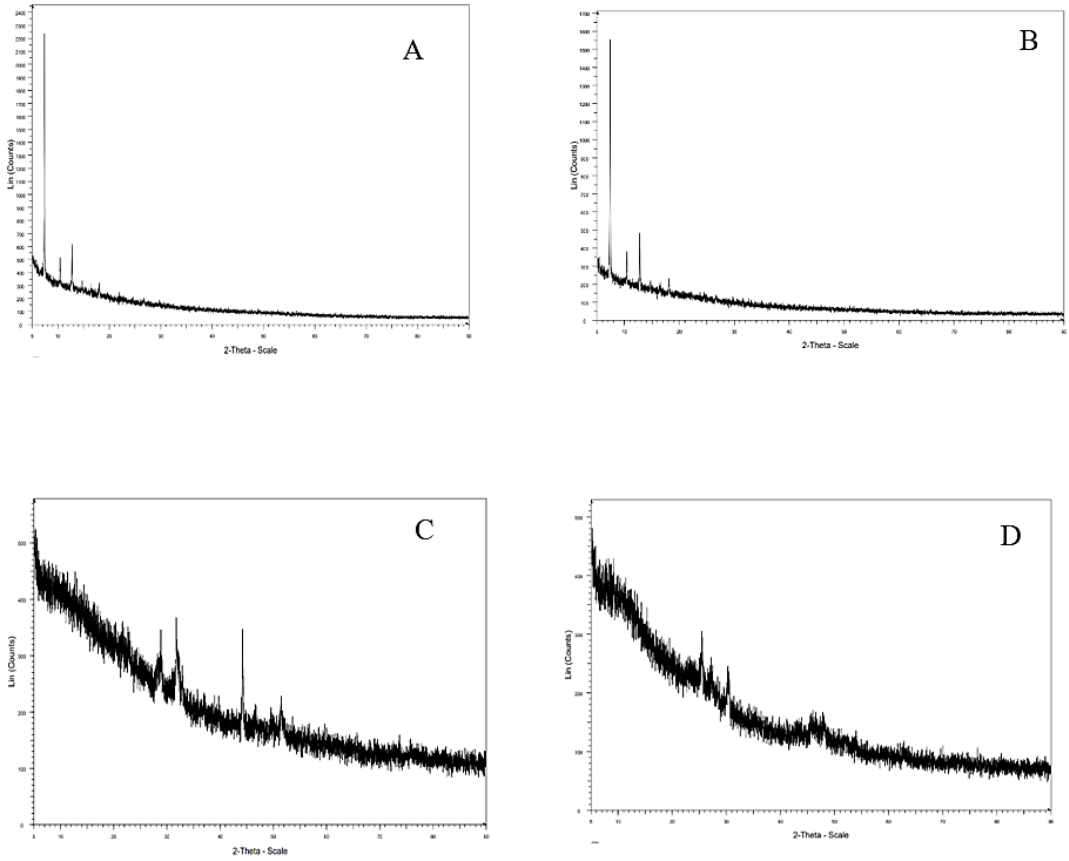

Figure 7. XRD patterns of the synthesized electrocatalysts: (A) ZIF-8@Gd-ZIF-67 precursor, (B) ZIF-8@Gd-ZIF-67@SiO_2 composite, (C) Gd-Co-N-PC after pyrolysis, and (D) Gd-Co-N-PC after HF treatment. Peaks corresponding to graphitic carbon and metallic cobalt confirm successful transformation into a conductive, catalytically active material

3.1.4. Raman Spectroscopy

Raman spectra (Figure 8) revealed the D and G bands characteristic of carbon materials. After HF washing, an increase in the I_D/I_G ratio from 0.953 to 1.015 indicated the creation of more defects and active sites, which can substantially enhance ORR catalytic performance[40, 41].

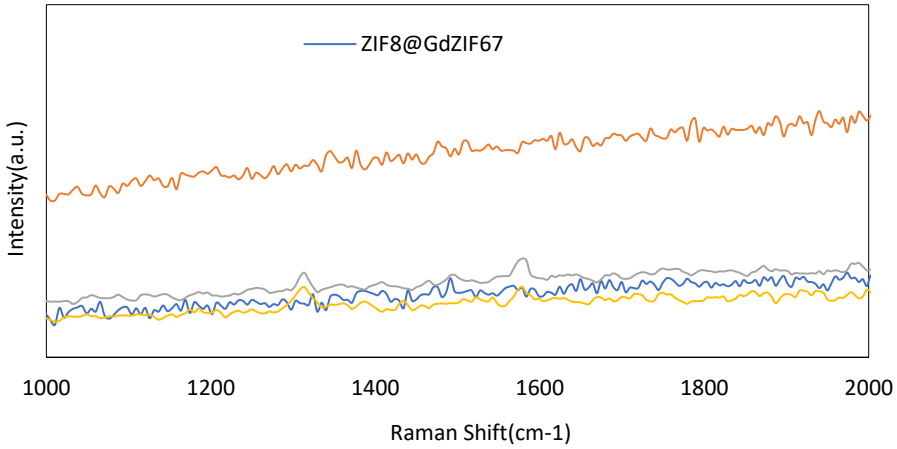

Figure 8. Raman spectra of the synthesized electrocatalysts, showing D and G bands. The increase in the I_D/I_G ratio after HF washing highlights the formation of more catalytically active defect sites

3.1.5. FTIR Spectroscopy

FTIR analysis (Figure 9) showed the presence of metal–oxygen bonds, C–N bonds, and carbonate groups. These results confirmed successful doping and carbonization, with the retention of critical functional groups that support high catalytic activity and stability.

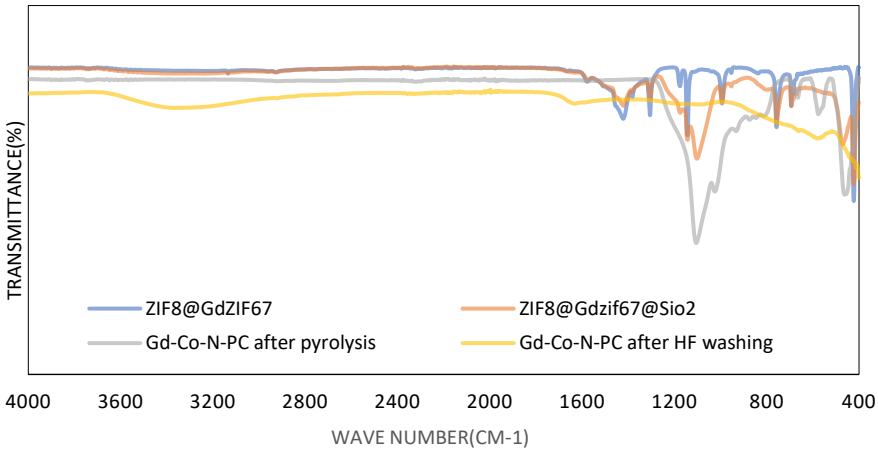

Figure 9. FTIR spectra of the prepared electrocatalysts, showing the presence of metal–oxygen, C–N, and carbonate functional groups, indicating successful doping and structural integrity following carbonization

3.2. Electrochemical Test Results of the Synthesized Catalysts

The electrochemical characteristics of the produced electrocatalysts were systematically examined in a 0.1 M KOH solution at ambient temperature (25 °C) using a series of techniques,

including cyclic voltammetry (CV), linear sweep voltammetry (LSV), and chronoamperometry. Additionally, Koutecky–Levich (K–L) analysis, based on LSV data, was used to determine the quantity of electrons exchanged in the oxygen reduction reaction (ORR), providing insight into the reaction pathway.

The electrocatalysts evaluated in this study included:

- ZIF-8@Gd-ZIF-67,
- ZIF-8@Gd-ZIF-67@SiO_2,
- Gd-Co-N-PC after pyrolysis (prior to HF treatment),
- Gd-Co-N-PC after HF washing.

The goal of this analysis was to determine which material exhibited the most promising ORR performance regarding onset potential, current density, electron transfer count, and operational stability, ultimately identifying the most efficient and durable catalyst for alkaline fuel cell applications.

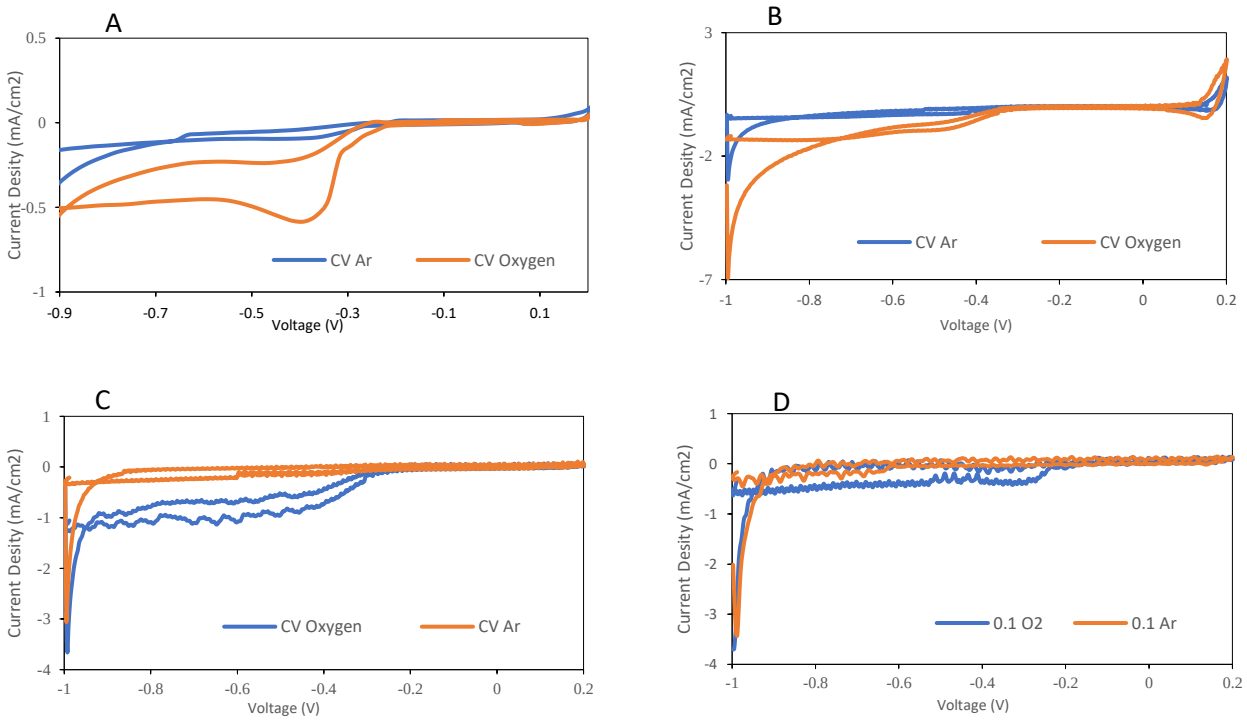

Figure 10. CV curves comparing ORR activity for (A) ZIF-8@Gd-ZIF-67, (B) ZIF-8@Gd-ZIF-67@SiO_2, (C) Gd-Co-N-PC after pyrolysis (before HF washing), and (D) Gd-Co-N-PC after HF washing

3.2.1. Cyclic Voltammetry (CV) Analysis

CV measurements were performed to investigate ORR activity. Prior to testing, Argon gas was passed through the electrolyte for 20 minutes to remove dissolved oxygen.. Under argon-

saturated conditions, no significant cathodic peaks were detected, confirming the absence of ORR. Upon oxygen saturation, all samples exhibited cathodic peaks indicative of ORR activity. Among them, Gd-Co-N-PC after HF washing demonstrated a sharper and more positively shifted cathodic peak, reflecting improved electrochemical kinetics and a higher density of active sites following the removal of the silica template (Figure 10, Figure 11).

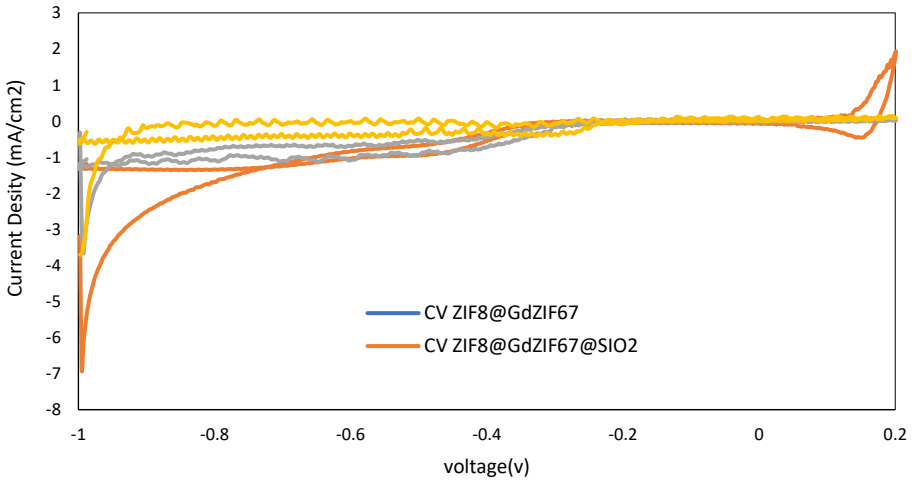

Figure 11. Comparative CV results of all synthesized electrocatalysts recorded at a rotation speed of 2500 rpm, highlighting the enhanced ORR performance of the Gd-Co-N-PC catalyst after HF treatment

3.2.2. Linear Sweep Voltammetry (LSV) Analysis

LSV tests were conducted in an oxygen-saturated electrolyte using a rotating disk electrode .(RDE) at varying speeds (400–2025 RPM). An Ag/AgCl electrode served as the reference Figures 12 and 13 present the LSV curves recorded at different rotation rates, which provide insight into the mass transport behavior and intrinsic catalytic activity of the prepared electrocatalysts. As expected, increasing the rotation speed enhances the convection-driven diffusion of oxygen molecules toward the electrode surface. This results in a pronounced increase in limiting current densities, consistent with the behavior predicted by the Koutecky–Levich (K–L) theory. Such trends confirm that the reaction kinetics are at least partially diffusion-controlled. Notably, the Gd-Co-N-PC catalyst after HF washing shows the most positive onset potential (compared to other samples), indicating a lower overpotential required to initiate the oxygen reduction reaction (ORR). This shift in onset potential suggests a more favorable adsorption of oxygen intermediates and enhanced electron transfer kinetics. Furthermore, the increased current density across the potential range implies that the active sites introduced or exposed by the HF treatment (likely through partial removal of inactive phases or surface cleaning) significantly contribute to ORR performance. Overall, the combination of improved onset potential and higher diffusion-limited current highlights the

Gd-Co-N-PC (HF-treated) as the most promising catalyst among the series, exhibiting both excellent intrinsic.

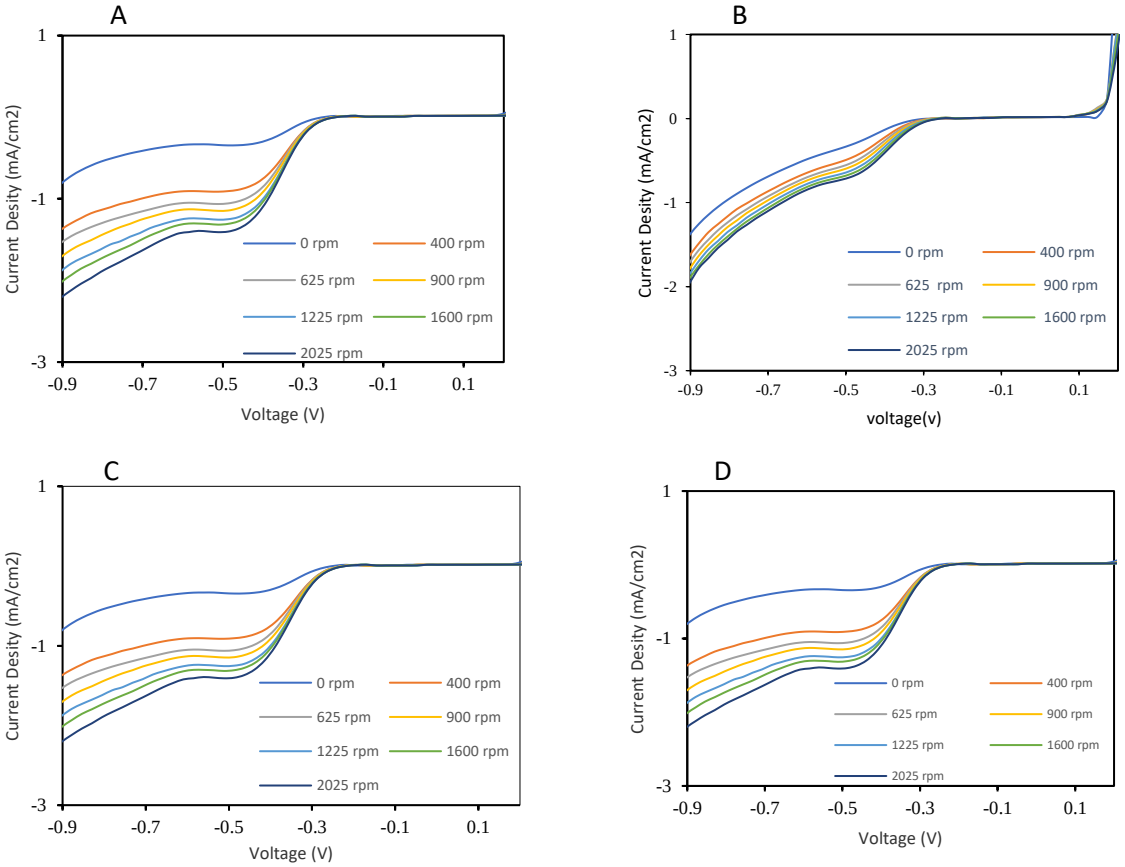

Figure 12. LSV curves showing ORR performance of (A) ZIF-8@Gd-ZIF-67, (B) ZIF-8@Gd-ZIF-67@SiO_2, (C) Gd-Co-N-PC after pyrolysis (before HF washing), and (D) Gd-Co-N-PC after HF washing at various rotation speeds (400–2025 RPM)

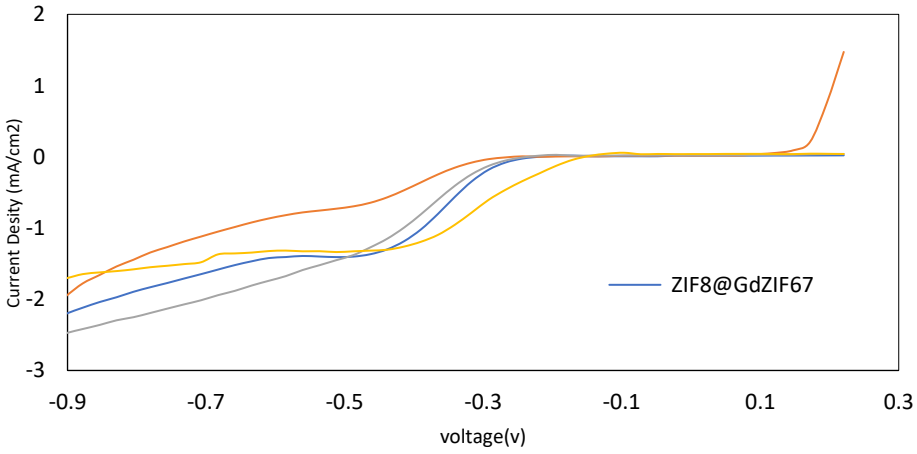

Figure 13. Comparison of LSV results for all synthesized electrocatalysts at 2500 RPM, highlighting the competitive performance of Gd-Co-N-PC after HF washing

As shown in Table 2, Gd-Co-N-PC displayed the greatest current density and onset potential following HF washing nearest to the positive axis among the synthesized catalysts. Its performance was remarkably close to that of the Pt/C 20% catalyst (–8.29 mA/cm² at +0.02 V vs. Ag/AgCl), demonstrating the success of the core–shell strategy, metal ion doping, and silica-assisted stabilization in enhancing ORR activity.

Table 2. Relationship between the synthesized electrocatalysts, the highest current density, and the closest onset potential

Synthesized Electrocatalyst	Onset Potential (V vs Ag/AgCl)
ZIF-8@Gd-ZIF-67	-0.34
ZIF-8@Gd-ZIF-67@SiO_2	-0.29
Gd-Co-N-PC after pyrolysis (before HF washing)	-0.26
Gd-Co-N-PC after HF washing	-0.12
Commercial Pt/C 20%	+0.02

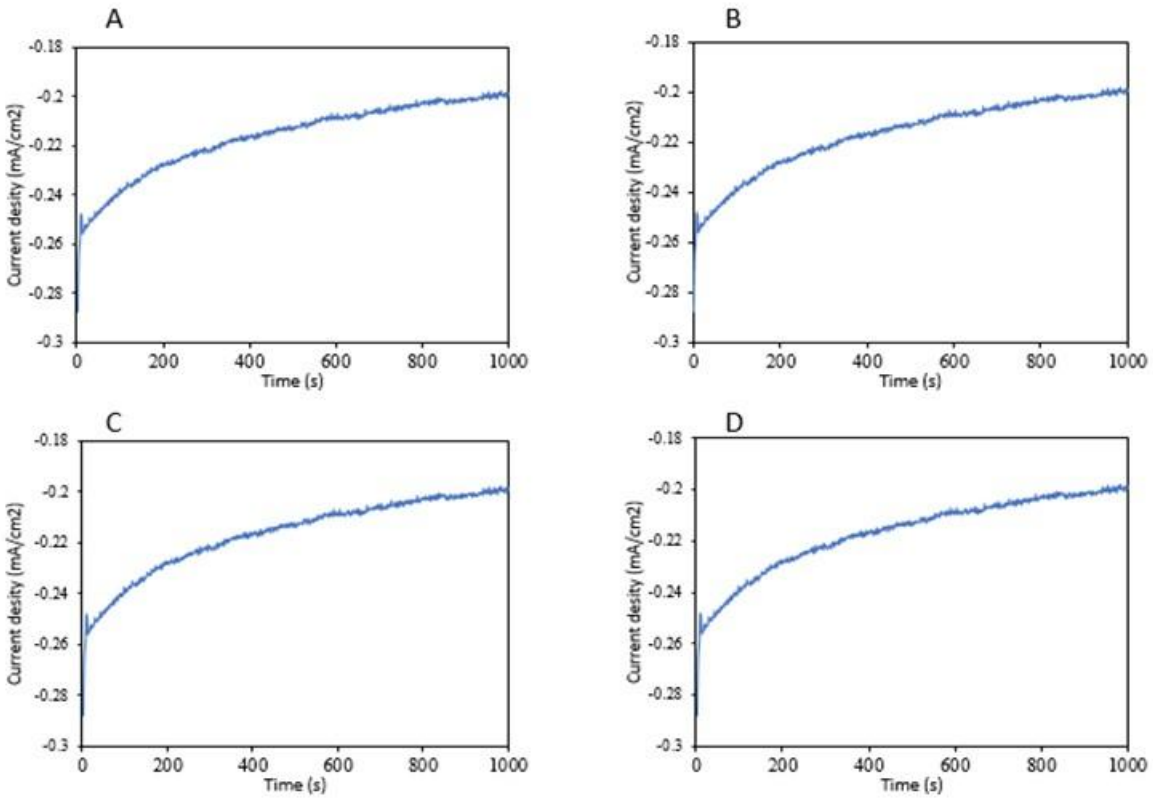

Figure 14. Chronoamperometric test outcomes for (A) ZIF-8@Gd-ZIF-67, (B) ZIF-8@Gd-ZIF-67@SiO_2, (C) Gd-Co-N-PC afte -pyrolysis (prior to HF washing), and (D) Gd-Co-N-PC after HF washing

3.2.3. Chronoamperometric Stability Test Results

Chronoamperometry was conducted at a constant potential of –0.4 V *vs.* Ag/AgCl over 4000 seconds in argon-saturated 0.1 M KOH at 25 °C [42]. As shown in Figure 14, the Gd-Co-N-PC sample subjected to HF washing rapidly achieved a steady-state current density, indicating fast stabilization of the electrode/electrolyte interface. Moreover, it exhibited excellent current retention with minimal degradation over the entire testing duration, highlighting its superior electrochemical durability. This stability can be attributed to the robust structure of the catalyst, the strong bonding between active sites and the carbon matrix, and the effective removal of inactive species via HF treatment, which collectively contribute to sustained catalytic performance under prolonged operation.

This excellent durability is attributed to:

- Strong interactions between hydroxide species and the carbon matrix,
- High specific surface areas,
- An increased number of accessible active sites,
- Suppression of nanoparticle aggregation during operation.

These features underline the suitability of the synthesized catalysts for long-term use in alkaline fuel cells and related energy conversion systems.

3.2.4. Koutecky–Levich (K–L) Analysis and Final Conclusion

The oxygen reduction reaction can proceed via either a four-electron pathway (direct reduction to OH^-) or a two-electron pathway (formation of peroxide intermediates). K–L analysis was used to determine the dominant reaction mechanism. The experimental data confirmed that pyrolysis, combined with Gd and Co doping, significantly enhanced the charge distribution, improving oxygen adsorption and ORR kinetics. Although MOFs inherently offer high surface areas and excellent adsorption capabilities, their limited electrical conductivity was effectively addressed through integration with carbon-based materials.

Table 3. Average amount of electrons transferred by the electrocatalysts synthesized in this study and their comparison with the commercial electrocatalyst%20 Pt/C

Electrocatalyst	Electron transfer number
ZIF8@Gdzif67	3.62
ZIF8@Gdzif67@sio_2	3.36
Gd-Co-N-PC after pyrolysis (before HF washing)	3.51
Gd-Co-N-PC after HF washing	3.69
% 20 Pt/C	3.76

K–L plots derived from the LSV results indicated that Gd-Co-N-PC after HF washing achieved an electron transfer number close to 3.69, approaching the ideal four-electron pathway, indicating highly efficient ORR behavior. In conclusion, the Gd-Co-N-PC electrocatalyst, synthesized through a strategy integrating MOF-derived nanostructuring, core–shell architecture, and silica protection, exhibits excellent catalytic activity, durability, and cost-effectiveness. These findings emphasize its potential as a favorable substitute for platinum-based catalysts in upcoming fuel cell applications.

4. CONCLUSION

Fuel cells represent one of the most promising alternatives to fossil fuel-based energy systems. The type of catalyst employed at the cathode and anode critically determines the overall performance and efficiency of fuel cells. Currently, platinum, a rare and expensive metal, remains the most widely used electrocatalyst; however, its high cost, limited availability, and durability issues have driven the search for alternative materials.

In this study, a series of electrocatalysts—namely ZIF-8@Gd-ZIF-67, ZIF-8@Gd-ZIF-67@SiO_2, Gd-Co-N-PC before HF washing, and Gd-Co-N-PC after HF washing—were successfully synthesized using hydrothermal methods. Their structural, morphological, and electrochemical properties were systematically evaluated through a combination of advanced characterization techniques, including X-ray diffraction (XRD), field emission scanning electron microscopy (FESEM), Fourier-transform infrared spectroscopy (FTIR), transmission electron microscopy (TEM), Raman spectroscopy, cyclic voltammetry (CV), linear sweep voltammetry (LSV), Koutecky–Levich (K–L) analysis, and chronoamperometry. The performance of the synthesized catalysts was directly in comparison to the commercial 20% Pt/C catalyst to assess their suitability for oxygen reduction reaction (ORR) applications. SEM analysis at various magnifications confirmed the uniform formation of metal–organic frameworks (MOFs) with nanometer-scale particle sizes. This morphology contributes to a high surface area-to-volume ratio, which is favorable for enhancing oxygen reduction reaction (ORR) kinetics. X-ray diffraction (XRD) patterns further validated the successful synthesis of the materials, with no evidence of impurity phases. Transmission electron microscopy (TEM) revealed well-defined polyhedral structures, consistent with the intended MOF architecture. Energy-dispersive X-ray spectroscopy (EDS) mapping demonstrated the homogeneous distribution of key elements carbon (C), nitrogen (N), oxygen (O), cobalt (Co), zinc (Zn), and gadolinium (Gd) throughout the composite. Additionally, FTIR and Raman spectroscopy confirmed the successful formation of carbon structures and effective nitrogen doping following pyrolysis under a nitrogen atmosphere at 900 °C. Electrochemical evaluations indicated that the Gd-Co-N-PC electrocatalyst after HF washing exhibited a near-four-electron ORR pathway, as evidenced by an electron transfer number of approximately 3.69. The cyclic voltammetry tests revealed clear ORR peaks under oxygen-saturated conditions, and LSV

results showed an onset potential of –0.12 V, nearing the performance of the commercial Pt/C catalyst at 0V. Chronoamperometric studies demonstrated that the synthesized catalysts maintained excellent stability over extended operational periods. These findings collectively demonstrate that the integration of carbon-based materials with metal–organic frameworks, combined with metal doping and silica coating strategies, significantly enhances the electrocatalytic performance and stability.

Consequently, the developed electrocatalysts present a promising, budget-friendly substitute for platinum-based systems in energy conversion and storage applications.

Some future works are recommended as follows:

1. Optimization of Mass Ratios

Conduct sensitivity analyses by varying the concentrations of ZIF-8@Gd-ZIF-67 and adjusting metal ratios to assess their influence on structural properties and ORR activity.

2. *Exploring Alternative MOFs and Lanthanides*

Investigate the synthesis and evaluation of different metal–organic frameworks and lanthanide-based systems, with a focus on performance under both alkaline and acidic conditions.

3. Pyrolysis Condition Analysis

Explore the effects of different pyrolysis temperatures (600–1000 °C) and atmospheres (nitrogen, argon, ammonia, etc.) on the structural and catalytic properties of the electrocatalysts.

4. Integration with Advanced Carbon Supports

Examine the incorporation of advanced carbon materials such as graphene oxide (GO), carbon nanotubes (CNTs), and layered double hydroxides (LDHs), either individually or in combination, to further enhance catalytic activity and stability.

5. Single-Cell Fuel Cell Testing

Fabricate membrane electrode assemblies (MEAs) incorporating the synthesized electrocatalysts and evaluate their performance in single-cell fuel cell systems. Testing under practical operating conditions, including power output, fuel utilization, and long-term durability, will provide critical validation of the materials' real-world applicability and scalability.

Declarations of interest

The authors declare no conflict of interest in this reported work.

REFERENCES

[1] B. Wang, L. Xu, G. Liu, P. Zhang, W. Zhu, J. Xia, and H. Li, J. Mater. Chem. A 5 (2017) 20170.

[2] H. Pourfarzad, M. Saremi, S. Khadem Jafari, R. Jazmi, and R. Badrnezhad, Anal. Bioanal. Electrochem. 14 (2022) 486.

[3] M. Mehrpooya, H. Ansarinasab, and S.A. Mousavi, Renew. Energy 172 (2021) 1314.

[4] D.K. Dang, and B. Zhou, J. Power Sources 623 (2024) 235475.

[5] M.S. Wilson, Google Patents (1993).

[6] B.G. Pollet, A.A. Franco, H. Su, H. Liang, and S. Pasupathi, Compend. Hydrog. Energy (2016) 3.

[7] M.M. Mench, Fuel Cell Engines, John Wiley & Sons (2008).

[8] P. Banoth, C. Kandula, and P. Kollu, ACS, Washington, DC (2022).

[9] T. Rasheed, K. Rizwan, M. Bilal, and H.M.N. Iqbal, Molecules 25 (2020) 1598.

[10] M. El Ouardi, H. Ait Ahsaine, M. Zbair, A. BaQais, and M. Saadi, Chemosphere 308 (2022) 136483.

[11] G. Zhong, D. Liu, and J. Zhang, J. Mater. Chem. A 6 (2018) 1887.

[12] Y. Liu, X. Zhou, Z. Jia, H. Wu, and G. Wu, Adv. Funct. Mater. 32 (2022) 2204499.

[13] A. Phan, C.J. Doonan, F.J. Uribe-Romo, C.B. Knobler, M. O'Keeffe, and O.M. Yaghi, Acc. Chem. Res. 43 (2009) 58.

[14] W. Xie, and F. Wan, Energy Convers. Manag. 198 (2019) 111922.

[15] M. Zhang, S. Miao, and B.-Q. Xu, Catal. Sci. Technol. 9 (2019) 4668.

[16] Z. Jia, M. Kong, B. Yu, Y. Ma, J. Pan, and G. Wu, J. Mater. Sci. Technol. 127 (2022) 153.

[17] S.A. Mousavi, and M. Mehrpooya, Energy 214 (2021) 119053.

[18] B. Chen, G. Ma, D. Kong, Y. Zhu, and Y. Xia, Carbon 95 (2015) 113.

[19] M.S. Esmaeili, M. Mehrpooya, and M.R. Ganjali, Int. J. Hydrog. Energy 97 (2025) 483.

[20] S. Bakhtavar, M. Mehrpooya, M. Manoochehri, and M. Karimkhani, Mater. Chem. Phys. 328 (2024) 129993.

[21] Z. Xue, J. Jiang, M.-G. Ma, M.-F. Li, and T. Mu, ACS Sustain. Chem. Eng. 5 (2017) 2623.

[22] S. Kumar, M. Singh, R. Pal, U.P. Azad, A.K. Singh, D.P. Singh, V. Ganesan, A.K. Singh, and R. Prakash, Int. J. Hydrog. Energy 46 (2021) 17163.

[23] S.A. Mousavi, M. Mehrpooya, and M.R. Ganjali, Mater. Chem. Phys. 320 (2024) 129394.

[24] L. Shang, H. Yu, X. Huang, T. Bian, R. Shi, Y. Zhao, G. I. N. Waterhouse, L.-Z. Wu, C.-H. Tung, and T. Zhang, Adv. Mater. 28 (2016) 1668.

[25] H. Kamali, M. Mehrpooya, S.A. Mousavi, and M.R. Ganjali, New J. Chem. 46 (2022) 18351.

[26] S.A. Mousavi, M. Mehrpooya, and M.R. Ganjali, J. Phys. Chem. Solids 202 (2025) 112684.
[27] I.L. Ikhioya, N. Alghamdi, S.E. Omeje, D.C. Ikeh, and R.N. Odoh, Chem. Inorg. Mater. 4 (2024) 100075.
[28] S. Liu, Z. Wang, S. Zhou, F. Yu, M. Yu, C.-Y. Chiang, W. Zhou, J. Zhao, and J. Qiu, Adv. Mater. 29 (2017) 1700874.
[29] B. Guo, J. Zhao, Y. Xu, X. Wen, X. Ren, X. Huang, S. Niu, Y. Dai, R. Gao, P. Xu, and S. Li, J. Am. Chem. Soc. 140 (2018) 2610.
[30] X. Liu, Y. Ma, Y. Cai, S. Hu, J. Chen, Z. Liu, and Z. Wang, RSC Adv. 11 (2021) 15722.
[31] S. Liu, Z. Wang, S. Zhou, F. Yu, M. Yu, C.-Y. Chiang, W. Zhou, J. Zhao, and J. Qiu, Adv. Mater. 29 (2017) 1700874.
[32] N. Bou-ydia, H. Atmani, M. Boulghallat, A. Jouaiti, and L. Laallam, Anal. Bioanal. Electrochem. 16 (2024) 206.
[33] S.G. Savari and S.J. Selvaraj, Anal. Bioanal. Electrochem. 16 (2024) 163.
[34] H. Pourfarzad and F. Torabi, Anal. Bioanal. Electrochem. 15 (2023) 318.
[35] D. Zhang, R. Ding, S. Shi, and Y. He, Int. J. Hydrog. Energy 48 (2023) 30391.
[36] S.A. Mousavi, M. Mehrpooya, and M.R. Ganjali, Int. J. Hydrog. Energy 51 (2024) 787.
[37] X.X. Wang, et al., Adv. Mater. 30 (2018) 1706758.
[38] S.A. Mousavi, M. Mehrpooya, and M.R. Ganjali, J. Phys. Chem. Solids 202 (2025) 112684.
[39] T. Wang, J. Zhuo, Y. Chen, K. Du, P. Papakonstantinou, Z. Zhu, Y. Shao, and M. Li, ChemCatChem 6 (2014) 1877.
[40] Z. Chen, X. Duan, W. Wei, S. Wang, and B.-J. Ni, J. Mater. Chem. A 7 (2019) 14971.
[41] K. Shen, X. Chen, J. Chen, and Y. Li, ACS Catal. 6 (2016) 5887.
[42] L. Yan, Y. Lin, X. Yu, W. Xu, T. Salas, H. Smallidge, M. Zhou, and H. Luo, ACS Appl. Mater. Interfaces 9 (2017) 23820.